2023 IEEE International Conference on Communications Workshops (ICC Workshops) | 979-8-3503-3307-7/23/$31.00 ©2023 IEEE | DOI: 10.1109/ICCWORKSHOPS57953.2023.10283590

Beyond 5G-assisted Automatic Guided Vehicles in Seaport Environments

Gianluca Torsoli*, Stefano Stracca†, Marzio Puleri†, Moe Z. Win‡, and Andrea Conti*

*Department of Engineering and CNIT, University of Ferrara, Via Saragat 1, 44122 Ferrara, Italy
(e-mail: gianluca.torsoli@unife.it, a.conti@ieee.org)
†Ericsson Research, Via Giuseppe Moruzzi 1, 56124 Pisa, Italy
(e-mail: stefano.stracca@ericsson.com, marzio.puleri@ericsson.com)
‡Laboratory for Information and Decision Systems, Massachusetts Institute of Technology, Cambridge, MA 02139 USA
(e-mail: moewin@mit.edu)

***Abstract*—Location awareness is vital for several fifth generation (5G) and beyond wireless applications. In particular, the use of 5G localization to assist or control automatic guided vehicles (AGVs) in seaport environments is a relevant use case conceived by the 3rd Generation Partnership Project (3GPP) standardization body. However, AGVs control systems require accurate localization, which is challenging in dynamic and cluttered environments like seaports. This paper proposes the use of soft information (SI)-based localization for providing location awareness to assist the motion of AGVs. The localization and navigation performance is determined considering the digital twin of a real seaport environment. Results show that SI-based localization can provide reliable AGVs navigation in 5G and beyond seaport environments.**

***Index Terms*—5G, autonomous vehicles, localization, seaport, digital twin**

Fig. 1. Picture of the digital twin of the seaport environment.

I. Introduction

Network localization and navigation is a fundamental enabler for several applications in fifth generation (5G) and beyond wireless networks [1]. Among the different 5G use cases (UCs) defined by the 3rd Generation Partnership Project (3GPP), accurate localization in maritime-related UCs is raising interest [2]. The localization information provided by the 5G network can be leveraged to enhance transportation efficiency, freight traceability, and shipment scheduling [3], [4]. In particular, the use of automatic guided vehicles (AGVs) is expected to greatly optimize seaport logistics operations. However, AGVs require accurate position information to perform collision avoidance and motion control, which is particularly difficult to achieve in seaport environments [2]. In fact, seaports are complex wireless environments, typically characterized by the wide presence of metallic containers which determine frequent non-line-of-sight (NLOS) conditions, and heavy multipath propagation.

AGVs can be deployed with two different navigation strategies, namely fixed-guided paths and open paths [5]. Navigation with fixed-guided paths refers to the use of a physical guidance (e.g., inductive guides on factory floors) to control the AGV movements. Such systems are highly reliable and often do not need positional information, however, they lack in terms of flexibility and have a significant infrastructure cost. On the contrary, AGVs with open paths can move freely in the environment, thus requiring accurate real-time localization. In such situations, the AGV position is conventionally estimated using radio frequency identification (RFID) sensors, laser sensors, cameras, or with the global navigation satellite system (GNSS) [6]. However, such technologies are not able to provide the flexibility and accuracy required for localization in highly dynamic and highly cluttered environments like seaports [7]. For example, cameras are limited by visual obstructions, while the GNSS is not able to provide accurate localization in indoor environments [8]. Moreover, these technologies require a dedicated infrastructure for AGV communication (e.g., based on the IEEE 802.11 standard [9]).

In this context, the use of private 5G networks for localization and communication is gaining importance [10]. In fact, 5G networks are able to overcome the limitations of the GNSS, providing accurate and ubiquitous localization with high flexibility and scalability [11]. Moreover, 5G networks can deliver ultra reliable low latency communication (URLLC) sharing the same infrastructure with localization. This is a key enabler to enhance 5G and beyond networks capabilities through the integrated sensing and communication (ISAC) paradigm [12]. Localization in cellular networks is currently performed through single-value estimate (SVE)-based algorithms. However, soft information (SI)-based localization was recently proposed for enhancing location awareness in 5G and beyond wireless networks [13]. Specifically, SI-based localization leverages machine learning techniques to provide a probabilistic description of the relationship among measurements, contextual information, and user equipment (UE) position [14]. The goal of this paper is to demonstrate 5G-assisted AGVs navigation in seaport environments. The key idea is to leverage SI-based localization for providing accurate location awareness to the AGV control system.

This paper advocates the use of SI-based localization in beyond 5G networks to assist the navigation of AGVs. Results are determined considering the digital twin of a real seaport environment. The key contributions of this paper can be summarized as follows:

- development of a SI-based localization method for seaport environments;
- characterization of the SI-based localization error via statistical modeling in 3GPP settings; and
- quantification of beyond 5G-assisted AGVs navigation performance considering the digital twin of a real seaport environment.

The remainder of the paper is organized as follows. Section II describes localization in 5G networks and SI-based localization; Section III describes the model for SI-based localization uncertainty in a seaport environment; Section IV describes the AGV navigation system; Section V presents the simulation environment and performance results for localization and navigation in the 3GPP framework; Finally, Section VI provides our conclusions.

Notations: a random vector and its realization are denoted by x and $\boldsymbol{x}$; a set is denoted by calligraphic fonts as $\mathcal{X}$; a matrix is denoted as $\boldsymbol{X}$ and its determinant as $|\boldsymbol{X}|$. The function $f_{\mathsf{x}}(\boldsymbol{x};\boldsymbol{\theta})$ indicates the probability distribution function (PDF) of a continous random vector x parametrized by $\boldsymbol{\theta}$;

II. Localization in 5G Networks

Localization aims to determine the position $\boldsymbol{p} \in \mathbb{R}^2$ of any UE based on a set of measurements exchanged with the gNodeBs (gNBs). Specifically, let $j \in \mathcal{N}_{\mathrm{b}} = \{1, 2, \dots, N_{\mathrm{b}}\}$ be the gNBs index where N_{b} is the number of gNBs in the scenario. Moreover, let $\{\hat{\boldsymbol{\theta}}_j\}_{j\in\mathcal{N}_{\mathrm{b}}}$ be a set of SVEs obtained from the gNBs. For example, in the following, $\hat{\boldsymbol{\theta}}_j = [\hat{\tau}_j, \hat{\alpha}_j]$ where $\hat{\tau}_j$ denotes a time-of-arrival (TOA) measurement and $\hat{\alpha}_j$ denotes an angle-of-departure (AOD) measurement [15]. According to 3GPP specifications for 5G localization, two reference signals (RSs), namely positioning reference signal (PRS) in downlink (DL) and sounding reference signal (SRS) in uplink (UL) can be used for localization [15]. The RSs can be transmitted in two frequency ranges, i.e., frequency range 1 (FR1) (central frequency below 7.125 GHz) and frequency range 2 (FR2) (central frequency between 24.25 and 52.6 GHz). In the case study presented in this paper, the AGV localization relies on the SVEs obtained from PRS transmission in FR1.

Existing approaches for TOA estimation in DL are based on the detection of the delay associated with the earliest peak (highest value) in the magnitude of the cross-correlation between the transmitted and the received PRS [16], [17]. The AOD is estimated based on multiple PRS transmissions with different steering vectors for the gNB antenna array. Specifically, the identification of the PRS transmission which determines the highest reference signal received power (RSRP) enables the estimation of the AOD [18].

The SI is composed of soft feature information (SFI) and soft context information (SCI) [14]. SFI refers to the ensemble of positional information associated with the measurements and can be divided into soft range information (SRI) (i.e., related to time or distance measurements) and soft angle information (SAI) (i.e., related to angle measurements). SCI encapsulates all the information associated with contextual data (e.g., digital maps and mobility models). In a non-Bayesian setting for 5G localization, the SFIs can be written as

$$\mathcal{L}_{\hat{\tau}}(\tau) \propto f_{\hat{\boldsymbol{\tau}}}(\hat{\tau};\tau) \tag{1a}$$
$$\mathcal{L}_{\hat{\alpha}}(\alpha) \propto f_{\hat{\boldsymbol{\alpha}}}(\hat{\alpha};\alpha) \tag{1b}$$

where (1a) refers to the SRI of TOA measurements and (1b) refers to the SAI of AOD measurements. The positional features τ and α denote the true TOA and the true AOD, respectively.

Let $\{\hat{\tau}_j\}_{j\in\mathcal{N}_{\mathrm{b}}}$ and $\{\hat{\alpha}_j\}_{j\in\mathcal{N}_{\mathrm{b}}}$ be two collections of independent measurements, then the position can be obtained through a maximum a posteriori estimation as

$$\hat{\boldsymbol{p}} = \arg\max_{\tilde{\boldsymbol{p}}} \left\{ \Phi_{\boldsymbol{\zeta}}(\tilde{\boldsymbol{p}}) \prod_{j\in\mathcal{N}_{\mathrm{b}}} \mathcal{L}_{\hat{\tau}_j}(\tau_j)\, \mathcal{L}_{\hat{\alpha}_j}(\alpha_j) \right\} \tag{2}$$

where $\Phi_{\boldsymbol{\zeta}}(\boldsymbol{p})$ is the SCI related to a contextual information $\boldsymbol{\zeta}$. Hereafter, $\boldsymbol{\zeta}$ refers to the knowledge of the environment digital map, thus the SCI is given by

$$\Phi_{\boldsymbol{\zeta}}(\boldsymbol{p}) = \begin{cases} 1/|\mathcal{M}| & \text{if } \boldsymbol{p} \in \mathcal{M} \\ 0 & \text{if } \boldsymbol{p} \notin \mathcal{M} \end{cases} \tag{3}$$

where $\mathcal{M}$ denotes the set of possible positions in the digital map and $|\mathcal{M}|$ denotes the number of elements in $\mathcal{M}$. Note that (2) considers both TOA and AOD measurements, hence the position can be always estimated without ambiguity even when a single gNB is available for localization.

Let $\hat{\theta}$ and θ denote a SVE and the positional feature, respectively (either TOA or AOD). The SFI is proportional to a generative model $f_{\hat{\boldsymbol{\theta}},\boldsymbol{\theta}}(\hat{\theta},\theta)$, i.e., an approximation of the joint probability distribution of the measurements $\hat{\theta}$ and positional features θ. In complex wireless environments, like seaports, the generative model cannot be determined a priori based on simple statistical relationships and it must be learned through a density estimation process. In particular, the generative model can be obtained fitting to a training dataset a Gaussian mixture model (GMM), whose parameters can be obtained through the expectation-maximization (EM) algorithm [19].

III. SI-based Localization Uncertainty Model

The modeling of localization uncertainty is fundamental to describe the localization accuracy that can be leveraged to assess the performance of different location-based services.

In particular, localization uncertainty models can be obtained fitting a 2-dimensional Gaussian distribution to the SI-based localization horizontal error on the two coordinates. Specifically, let $\boldsymbol{e} = [e_x, e_y]^{\mathrm{T}} \in \mathbb{R}^2$ be the vector containing the localization error, where e_x and e_y denote the error on the x and on the y coordinate. Then, the uncertainty model is given by

$$\hat{f}_{\mathbf{e}}(\boldsymbol{e};\boldsymbol{\mu},\boldsymbol{\Sigma}) = \frac{1}{2\pi|\boldsymbol{\Sigma}|^{\frac{1}{2}}} \exp\left\{\frac{-(\boldsymbol{e}-\boldsymbol{\mu})^{\mathrm{T}}\boldsymbol{\Sigma}^{-1}(\boldsymbol{e}-\boldsymbol{\mu})}{2}\right\}. \quad (4)$$

Based on a collection $\{\boldsymbol{e}^{(n)}\}_{n=1}^{N_{\mathrm{e}}}$ of localization errors, the parameters of (4) are obtained as

$$\hat{\boldsymbol{\mu}} = \frac{1}{N_{\mathrm{e}}}\sum_{n=1}^{N_{\mathrm{e}}} \boldsymbol{e}^{(n)} \quad (5a)$$

$$\hat{\boldsymbol{\Sigma}} = \frac{1}{N_{\mathrm{e}}-1}\sum_{n=1}^{N_{\mathrm{e}}} (\boldsymbol{e}^{(n)}-\hat{\boldsymbol{\mu}})(\boldsymbol{e}^{(n)}-\hat{\boldsymbol{\mu}})^{\mathrm{T}}. \quad (5b)$$

The accuracy of the model is evaluated in the following via the Jensen-Shannon divergence (JSD) between the fit model and the empirical probability mass function (EPMF) of $\{\boldsymbol{e}^{(n)}\}_{n=1}^{N_{\mathrm{e}}}$. Specifically, the lower the JSD, the higher the model accuracy [20].

IV. AGV Trajectory Planning and Motion Control

The system for the AGV trajectory planning and motion control operates in two phases:

1) an offline phase where a task is assigned to the AGV and a trajectory for completing that task is computed; and
2) an online phase where the 5G network is used for providing location awareness to the AGV motion control system via SI-based localization.

The AGV trajectories are planned based on the tasks assigned to the AGV. Each task is identified by the AGV initial position $\boldsymbol{x}_{\mathrm{i}}$ (e.g., a parking area), the target position $\boldsymbol{x}_{\mathrm{t}}$ (e.g., the location of freights to pick), and the destination position $\boldsymbol{x}_{\mathrm{d}}$. Then, the trajectories between $\boldsymbol{x}_{\mathrm{i}}$ and $\boldsymbol{x}_{\mathrm{t}}$, and between $\boldsymbol{x}_{\mathrm{t}}$ and $\boldsymbol{x}_{\mathrm{d}}$ are planned using the $A*$ algorithm [21]. Specifically, let $\boldsymbol{x}_1$ and $\boldsymbol{x}_2$ denote a generic starting and final position, respectively. Then, the $A*$ algorithm performs a graph search that determines the AGV trajectory by evaluating

$$\hat{c}(\boldsymbol{x};\boldsymbol{x}_1,\boldsymbol{x}_2) = g(\boldsymbol{x};\boldsymbol{x}_1) + \hat{d}(\boldsymbol{x};\boldsymbol{x}_2) \quad (6)$$

where $g(\boldsymbol{x};\boldsymbol{x}_1)$ is the distance traveled by the AGV from the starting position $\boldsymbol{x}_1$ to $\boldsymbol{x}$, and $\hat{d}(\boldsymbol{x};\boldsymbol{x}_2)$ is the euclidean distance between $\boldsymbol{x}$ and the final position $\boldsymbol{x}_2$. Since $\hat{d}(\boldsymbol{x};\boldsymbol{x}_2)$ is an admissible heuristic (i.e., it never overestimates the cost of reaching the destination) the $A*$ algorithm is proven to provide an optimal solution [21]. The trajectory planning performed by the $A*$ algorithm can be adapted to consider prior information (including the environment digital map in (3) and the position of known obstacles), by constraining the set of possible subgraphs at each $\boldsymbol{x}$ [21].

Once the AGV trajectory is computed, the AGV motion control determines the next AGV movement based on the feedback provided by SI-based 5G localization. In particular, here the AGV implements a non-linear fuzzy controller to guarantee a fast step response with a small overshoot for both long and short movements [22].

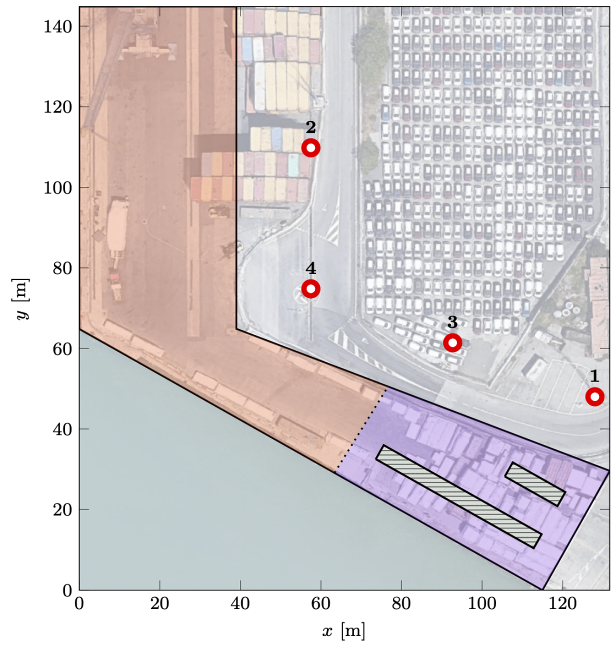

Fig. 2. Map of the seaport environment used as a reference for the digital twin located in Livorno, Italy. The red annuluses denote the gNBs positions while the hatched rectangles denote obstacles that determine NLOS conditions. The violet background identifies the storage area while the orange background identifies the shuttling area. The coordinates on the axis are in meters.

V. Case Studies

This section evaluates 5G-assisted AGV localization and navigation performance in the digital twin of a real seaport environment located in Livorno, Italy. The map of the real seaport environment used as a reference is reported in Fig. 2

A. Seaport digital twin

The digital twin is built using the professional Unity 3D game engine [23] (see an example image in Fig. 1). The freight inventory, the pending AGV tasks, and obstacle information are stored in a MySQL relational database. Such database is connected with an expert system made with C language integrated production system (CLIPS) [24] which determines the tasks the AGV has to accomplish and provides the corresponding data to the $A*$ algorithm for trajectory planning. Moreover, the developed digital twin can be explored through a virtual reality headset to evaluate firsthand the quality of AGV navigation [25].

B. SI-based localization performance

In absence of a standardized 3GPP channel model for seaport environments, the cluttered area at the bottom of the environment, hereafter referred to as storage, is modeled as a 3GPP 38.901 indoor factory (InF)-SH scenario, while the open area on the top, hereafter referred to as shuttling, is modeled

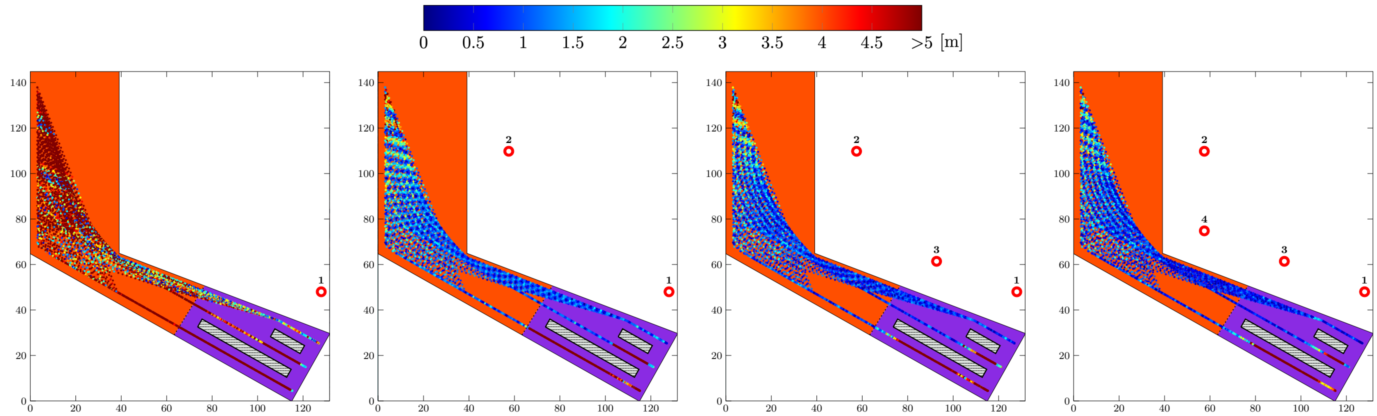

(a) 1 gNB (b) 2 gNBs (c) 3 gNBs (d) 4 gNBs

Fig. 3. Spatial distribution of the horizontal localization error for SI-based localization for some samples of the AGV trajectories with different gNB deployments. The coordinates on the axis and the magnitude of the localization error are in meters.

as a 3GPP 38.901 rural macro (RMa) scenario [26]. Such scenarios exhibit similar propagation conditions with respect to the ones that are expected in the two areas of the real seaport environment. The gNBs are deployed as in Fig. 2 and all their parameters are set according to the specifications for the 3GPP 38.901 RMa scenario in FR1 [26]. The NLOS conditions for the gNBs are obtained geometrically considering the position of the obstacles as in Fig. 2. The AGV is equipped with an omnidirectional antenna. The DL-TOA and AOD are obtained through the downlink transmission of the PRS in FR1 with a central frequency of 4 GHz and a bandwidth of 100 MHz.

To validate the localization performance, 120 AGV tasks were generated and the corresponding trajectories were planned. The AGV is simulated with a variable speed from 0 to $2.8\,\mathrm{m/s}$, and the trajectories were sampled every $0.5\,\mathrm{s}$ to obtain trajectory snapshots. For each snapshot, the wireless channel instantiations are simulated using the QuaDRiGa wireless channel simulator [27]. Specifically, the wireless channel instantiations are generated considering the trajectory spatial consistency and the AGV movement speed. The trajectories are then divided through 2-fold cross-validation [19]. For each fold, the training data are used for the estimation of both DL-TOA and AOD generative models with $N_{\mathrm{M}} = 6$ Gaussian components. The position is estimated via SI according to (2), where the SCI refers to the seaport environment digital map.

Fig. 3 shows the spatial distribution of the horizontal localization error. It can be observed that in the storage area the localization performance is worse with respect to the shuttling area for all the gNB deployment configurations.

Fig. 4 shows the empirical cumulative distribution function (ECDF) of the horizontal localization error for SI-based localization with different gNBs settings in the two areas of the seaport environment, as well as in the complete seaport environment. It can be observed that a deployment with a single gNB provides unsatisfactory localization performance. However, increasing the number of gNBs drastically improves localization performance both in the shuttling and in the storage area. For example, considering a deployment with 4 gNBs, at the 90th percentile the error is below 1.5 m for the shuttling area and around 10 m in the storage area.

Fig. 5 shows the ECDF of the horizontal localization error for SI-based localization with various numbers of gNBs in LOS conditions.[1] It can be observed that increasing the number of LOS gNBs improves the localization performance. It can also be observed that by increasing the number of gNB deployed in the seaport environment the performance improves even with the same number of LOS gNBs, hence NLOS gNBs also contribute to localization accuracy due to the use of the SI-based approach.

C. Localization uncertainty models in the 3GPP setting

Localization uncertainty models are obtained according to Sec. III evaluating a collection of localization errors obtained from 120 AGV trajectories in the seaport environment. In particular different models are determined for the shuttling and the storage areas with different numbers of gNB deployed. The models obtained are reported in Table I. In addition, the JSD, denoted by $\mathbb{D}_{\mathrm{JS}}\{\hat{f}_{\mathbf{e}}(e)\}$, is reported for each model. The low values of JSD denote the high accuracy of the models.

D. AGV navigation performance

To evaluate the AGV navigation performance, 64 tasks were generated and the corresponding trajectories were planned. The AGV starts moving following the planned trajectory, and every $0.5\,\mathrm{s}$ a new estimated AGV position is provided to the AGV motion control system. The AGV position is obtained by adding to the real position of the AGV in the environment a localization error obtained from the SI-based localization error models in Table I. No additional information on the uncertainty of the estimated position is provided to the AGV control system to improve navigation accuracy.

[1]The results are reported only if a significative number of snapshots are available to infer an ECDF.

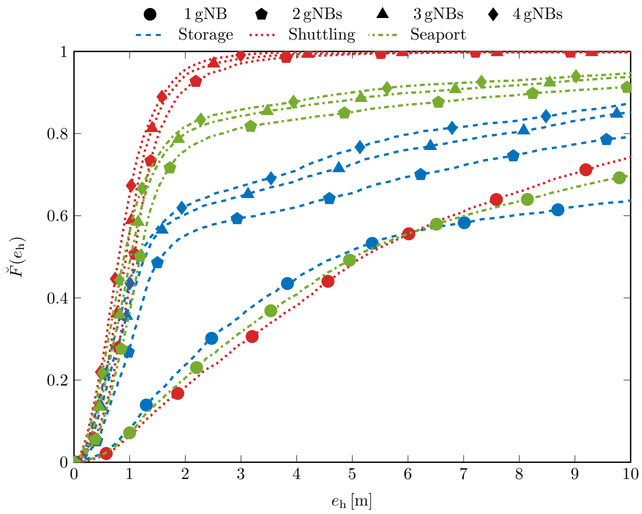

Fig. 4. ECDF of the SI-based localization error in the different areas of the seaport scenario.

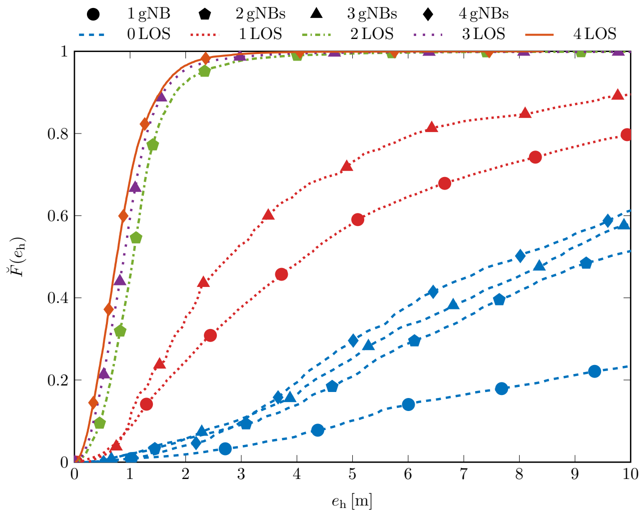

Fig. 5. ECDF of the SI-based localization error based on the number of LOS links between the AGV and the gNBs.

Fig. 6 shows the ECDF of AGV navigation performance for the gNBs deployment which provides the best localization performance (i.e., the deployment of 4 gNBs). It can be observed that sub-meter AGV navigation accuracy is achieved in both the storage and the shuttling areas for around the 60% of the cases, despite the different localization performance achievable in the two areas. Moreover, it can be observed that at the 90th percentile, the navigation error is around 2 m in both areas. Finally, it can be noticed that the AGV navigation error is below 3 m in all the cases considered. An example of AGV navigation, with a comparison to the planned trajectory, is reported in Fig. 7.

VI. Conclusion

This paper demonstrated the capability of soft information (SI)-based localization to assist automatic guided vehicle (AGV) navigation in fifth generation (5G) and beyond seaport scenarios. The accuracy of localization is fundamental to enable reliable AGV navigation. Extensive simulations compliant with 3rd Generation Partnership Project (3GPP) specifications were performed in the digital twin of a real seaport environment to characterize AGVs localization and navigation accuracy, as well as to provide accurate localization uncertainty models that can be leveraged to assess the performance of location-based services. Results show that the SI-based approach provides high localization accuracy to enable reliable AGV navigation, even with a reduced number of gNodeBs (gNBs) available for localization. Such results represent a step towards achieving 5G-assisted AGV navigation in seaport environments.

Acknowledgment

The fundamental research described in this paper was supported, in part, by the European Union's Horizon 2020 Research and Innovation Programme under Grant 871249, in part, by the Office of Naval Research under Grant N62909-22-1-2009, and, in part, by the National Science Foundation under Grant 2148251.

TABLE I
Parameters of the localization uncertainty models for the two areas of the seaport environment [m]

gNBs	Storage	Shuttling
1	$\hat{\boldsymbol{\mu}} = [-2.760, 1.441]$ $\hat{\boldsymbol{\Sigma}} = \begin{bmatrix} 161.576 & -99.774 \\ -99.774 & 115.658 \end{bmatrix}$ $\mathbb{D}_{\mathrm{JS}}\{\hat{f}_{\mathbf{e}}(\boldsymbol{e})\} = 0.0043$	$\hat{\boldsymbol{\mu}} = [-0.635, -1.962]$ $\hat{\boldsymbol{\Sigma}} = \begin{bmatrix} 9.092 & 19.319 \\ 19.319 & 89.646 \end{bmatrix}$ $\mathbb{D}_{\mathrm{JS}}\{\hat{f}_{\mathbf{e}}(\boldsymbol{e})\} = 0.0021$
2	$\hat{\boldsymbol{\mu}} = [0.7970, -1.212]$ $\hat{\boldsymbol{\Sigma}} = \begin{bmatrix} 45.948 & -4.396 \\ -4.396 & 13.410 \end{bmatrix}$ $\mathbb{D}_{\mathrm{JS}}\{\hat{f}_{\mathbf{e}}(\boldsymbol{e})\} = 0.0550$	$\hat{\boldsymbol{\mu}} = [-0.008, -0.034]$ $\hat{\boldsymbol{\Sigma}} = \begin{bmatrix} 0.653 & 0.156 \\ 0.156 & 1.852 \end{bmatrix}$ $\mathbb{D}_{\mathrm{JS}}\{\hat{f}_{\mathbf{e}}(\boldsymbol{e})\} = 0.0492$
3	$\hat{\boldsymbol{\mu}} = [0.093, -1.172]$ $\hat{\boldsymbol{\Sigma}} = \begin{bmatrix} 31.278 & -8.277 \\ -8.277 & 11.653 \end{bmatrix}$ $\mathbb{D}_{\mathrm{JS}}\{\hat{f}_{\mathbf{e}}(\boldsymbol{e})\} = 0.0531$	$\hat{\boldsymbol{\mu}} = [0.007, -0.074]$ $\hat{\boldsymbol{\Sigma}} = \begin{bmatrix} 0.984 & -1.073 \\ -1.073 & 3.547 \end{bmatrix}$ $\mathbb{D}_{\mathrm{JS}}\{\hat{f}_{\mathbf{e}}(\boldsymbol{e})\} = 0.0407$
4	$\hat{\boldsymbol{\mu}} = [0.916, -0.955]$ $\hat{\boldsymbol{\Sigma}} = \begin{bmatrix} 25.730 & -3.141 \\ -3.141 & 7.896 \end{bmatrix}$ $\mathbb{D}_{\mathrm{JS}}\{\hat{f}_{\mathbf{e}}(\boldsymbol{e})\} = 0.0804$	$\hat{\boldsymbol{\mu}} = [-0.001, -0.061]$ $\hat{\boldsymbol{\Sigma}} = \begin{bmatrix} 0.507 & -0.221 \\ -0.221 & 1.328 \end{bmatrix}$ $\mathbb{D}_{\mathrm{JS}}\{\hat{f}_{\mathbf{e}}(\boldsymbol{e})\} = 0.0667$

References

[1] M. Z. Win *et al.*, "Network localization and navigation via cooperation," *IEEE Commun. Mag.*, vol. 49, no. 5, pp. 56–62, May 2011.

[2] *Technical Specification Group Radio Access Network; Technical Specification Group Services and System Aspects; Study on positioning use cases*, 3GPP™ Std. TR 22.872 V16.1.0, Sept. 2018, Release 16.

[3] "Empowering vertical industries through 5G networks - current status and future trends," 5GPP™ Aug. 2020, version 1.0.

[4] M. Sadiq *et al.*, "Future greener seaports: A review of new infrastructure, challenges, and energy efficiency measures," *IEEE Access*, vol. 9, pp. 75 568–75 587, 2021.

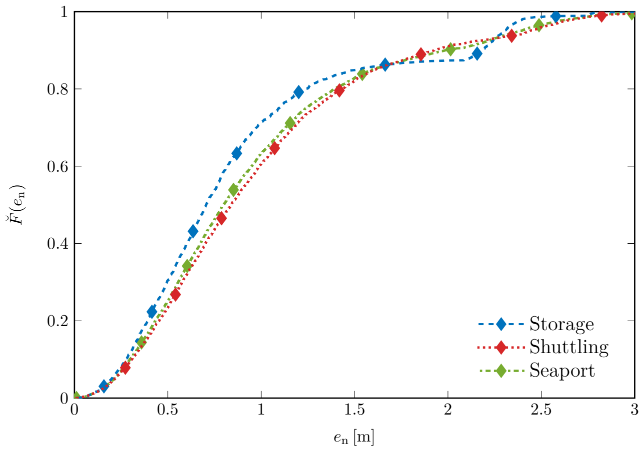

Fig. 6. ECDF of the AGV navigation error considering 4 gNBs available for localization in the different areas of the seaport environments.

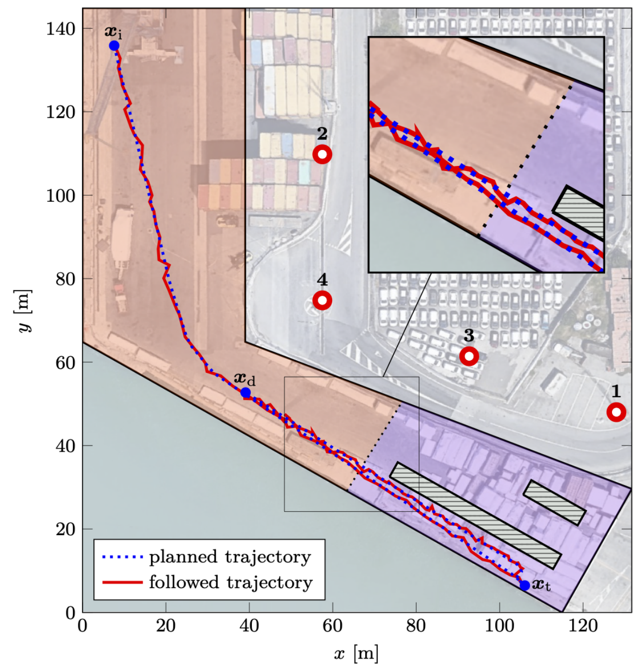

Fig. 7. Example of trajectory followed by the AGV in the seaport environment compared to the planned trajectory

[5] A. Fellan, C. Schellenberger, M. Zimmermann, and H. D. Schotten, "Enabling communication technologies for automated unmanned vehicles in Industry 4.0," in *Proc. IEEE Int. Conf. on Inform. and Commun. Technol. Conv. (ICTC)*, Jeju Island, South Korea, 2018, pp. 171–176.

[6] L. Lynch, T. Newe, J. Clifford, J. Coleman, J. Walsh, and D. Toal, "Automated ground vehicle (AGV) and sensor technologies - a review," in *Proc. Int. Conf. on Sensing Technol. (ICST)*, Limerick, Ireland, 2018, pp. 347–352.

[7] Y. Yang, M. Zhong, H. Yao, F. Yu, X. Fu, and O. Postolache, "Internet of things for smart ports: Technologies and challenges," *IEEE Instrum. Meas. Mag.*, vol. 21, no. 1, pp. 34–43, 2018.

[8] L. Chen *et al.*, "Robustness, security and privacy in location-based services for future IoT: A survey," *IEEE Access*, vol. 5, pp. 8956–8977, 2017.

[9] L. Seno, G. Cena, S. Scanzio, A. Valenzano, and C. Zunino, "Enhancing communication determinism in Wi-Fi networks for soft real-time industrial applications," *IEEE Trans. Ind. Informat.*, vol. 13, no. 2, pp. 866–876, 2017.

[10] M. Wen *et al.*, "Private 5G networks: Concepts, architectures, and research landscape," *IEEE J. Sel. Topics Signal Process.*, vol. 16, no. 1, pp. 7–25, Jan. 2022.

[11] S. Dwivedi *et al.*, "Positioning in 5G networks," *IEEE Commun. Mag.*, vol. 59, no. 11, pp. 38–44, Nov. 2021.

[12] G. Kwon, A. Conti, H. Park, and M. Z. Win, "Joint communication and localization in millimeter wave networks," *IEEE J. Sel. Topics Signal Process.*, vol. 15, no. 6, pp. 1439–1454, 2021.

[13] A. Conti *et al.*, "Location awareness in beyond 5G networks," *IEEE Commun. Mag.*, vol. 59, no. 11, pp. 22–27, Nov. 2021.

[14] A. Conti, S. Mazuelas, S. Bartoletti, W. C. Lindsey, and M. Z. Win, "Soft information for localization-of-things," *Proc. IEEE*, vol. 107, no. 11, pp. 2240–2264, Nov. 2019.

[15] *Technical Specification Group Radio Access Network; NG Radio Access Network (NG-RAN); Stage 2 functional specification of User Equipment (UE) positioning in NG-RAN*, 3GPP™ Std. TS 38.305 V17.0.0, Mar. 2022, Release 17.

[16] I. Guvenc and C.-C. Chong, "A survey on TOA based wireless localization and NLOS mitigation techniques," *IEEE Commun. Surveys Tuts.*, vol. 11, no. 3, pp. 107–124, 2009.

[17] G. Torsoli, M. Z. Win, and A. Conti, "Selection of reference base station for TDOA-based localization in 5G and beyond IIoT," in *Proc. IEEE Workshop, Global. Telecommun. Conf.*, Rio de Janeiro, Brazil, Dec. 2022.

[18] *Technical Specification Group Radio Access Network; NG Radio Access Network (NG-RAN); Stage 2 functional specification of User Equipment (UE) positioning in NG-RAN*, 3GPP™ Std. TS 38.305 V17.3.0, Dec. 2022, Release 17.

[19] C. M. Bishop, *Pattern Recognition and Machine Learning*. New York, NY, USA: Springer, 2006.

[20] J. Lin, "Divergence measures based on the Shannon entropy," *IEEE Trans. Inf. Theory*, vol. 37, no. 1, pp. 145–151, 1991.

[21] P. E. Hart, N. J. Nilsson, and B. Raphael, "A formal basis for the heuristic determination of minimum cost paths," *IEEE Trans. Syst. Sci. Cybern.*, vol. 4, no. 2, pp. 100–107, 1968.

[22] K. M. Passino and S. Yurkovich, *Fuzzy Control*, 1st ed. USA: Addison-Wesley Longman Publishing Co., Inc., 1997.

[23] A. Juliani *et al.*, "Unity: A general platform for intelligent agents," *arXiv:1809.02627*, Sept. 2018.

[24] J. C. Giarratano and G. D. Riley, *Expert Systems: Principles and Programming*. USA: Brooks/Cole Publishing Co., 2005.

[25] LOCUS Project, "Deliverable D 6.1: Detailed requirements from scenarios and application specification," Available at https://www.locus-project.eu/results/deliverables/, Jun. 2021.

[26] *Technical Specification Group Radio Access Network; Study on channel model for frequencies from 0.5 to 100 GHz*, 3rd Generation Partnership Project 3GPP™ TR 38.901 V17.0.0, Mar. 2022, Release 17.

[27] S. Jaeckel, L. Raschkowski, K. Börner, and L. Thiele, "QuaDRiGa: A 3-D multi-cell channel model with time evolution for enabling virtual field trials," *IEEE Trans. Antennas Propag.*, vol. 62, no. 6, pp. 3242–3256, 2014.